Investigating Aerodynamics in RC Vehicles: Comparing Sensor Data Across Diverse Shapes

University of Turku
Department of Computing
Master of Science (Tech) Thesis
Robotics and Autonomous Systems
August 2025
Michalis Iona

Supervisors:
Adjunct Professor Hashem Haghbayan
Professor Juha Plosila
MSc Tech. Abdul Malik

UNIVERSITY OF TURKU
Department of Computing

Michalis Iona: Investigating Aerodynamics in RC Vehicles: Comparing Sensor Data Across Diverse Shapes

Master of Science (Tech) Thesis, 54 p.
Robotics and Autonomous Systems
August 2025

This thesis investigates different shapes with various angles on front and rear placed on top of a robot, aiming to gather different data from various sensors placed around the shape, while experiencing considerable air resistance in different trajectories it travels. Each shape has a definitive incline and slope angle which was chosen according to the popular day-to-day vehicles used. A total of eight sensors were used by placing them in key positions surrounding the robot, with each in purpose of tracking the aerodynamic behaviour depending on the terrain and air friction it faces. One flow sensor on each side of the vehicle, two pressure sensors placed on top and front and one force sensor in the frontal area of the vehicle. Subject to the angular use of incline and slope of each shape, all these sensors output various data, while also taking into consideration the current environmental and weather condition when testing. A track with various turns and straights, which would be taken in different speeds, was chosen for the output of different data, depending on how tight the turns would be. The vehicle would be able to accompany results and understand how much drag, lift and grip each shape would have when taking those specific corners. As a result, printed shapes were designed and put on top of the vehicle with sensors connected to the Jetson Nano, where live data can be seen through a terminal and saved into spreadsheet format. The data around the track is captured in a graphical manner by timestamping each corner whilst simultaneously comparing all angles. Therefore, the knowledge can be used to reconfigure the robot based on what track it would be suitable for. The results obtained by the experiments of different applied angles, output a huge difference in airflow, depending on what part of the track the vehicle is at. The 90° provided much more downforce to the vehicles flow, whereas the lowest angle at 22.5° showed a minimal drag, which was advantageous in top speed straights. An increase of 62% of air friction can be found when comparing the 22.5° and 90°, respectively.

Keywords: aerodynamics , sensors, data, angles, motion, force, pressure, airflow

Contents

List of Figures

List of Tables

List of Acronyms

CFD - Computational Fluid Dynamics

3D - Three Dimensional

I²C - Inter-Integrated Circuit

RC - Remote Control

UART - Universal Asynchronous Receiver / Transmitter

SDA - Serial Data Line

SCL - Serial Clock Line

GPS - Global Positioning System

ADC - Analog to Digital Converter

SUV - Sport Utility Vehicle

CSV - Comma-Separated Values

1 Introduction

Aerodynamics research plays a crucial and important role when it comes to modern vehicle design, impacting efficiency, stability, and performance across a wide range of applications. This research project aims to investigate the aerodynamic behaviour of a remote controlled vehicle fitted with various shapes mounted on its surface, each characterized by unique angles of inclination and slopping trails. By analysing which geometric variations influence airflow, drag and lift, this research study seeks to identify the shape that optimizes aerodynamic performance for specific purposes. Unlike using a conventional approach that relies heavily on CFD simulations, this project adopts a hands-on, experimental methodology to foster a deeper understanding of aerodynamic principles through direct measurements and analysis.

During Chapter 2, a thorough research on the background of aerodynamics and its principles is discussed. Theoretical equations and background research on fluid dynamics, sensor functionality, environmental conditions, while also understanding the importance of flow trajectories in certain angles, is thoroughly looked upon to prepare and provide reasoning in my practical approach in testing different angular shapes placed on top of the vehicle. Each flow trajectory becomes unique when considering the design approach of different shapes. Distinctive environmental factors matter when checking the data, especially during testing phase, whenever high wind or low temperatures are in place. The three sensors selected for this research

were used to obtain the required data, which are thoroughly described and placed in positions which the author found key, to understand further how motion with different angles work upon.

The choice of the specific angles were pre-determined from using real life models from different types of vehicles where for example, a sports vehicle is usually with an angular incline of 22.5°, and a van is from a 90°.

The experimental framework is built around the usage of Jetson Nano in acquiring robust data, by utilizing an array of sensors with correct positioning to capture aerodynamic parameters. A force sensor is employed to measure the drag and lift forces exerted on the front of the vehicle as it moves, which can show how each shape affects resistance and vertical forces. Multiple flow sensors and pressure sensors are placed around the shape of the vehicle to capture patterns of turbulence or laminar flow and variations in air pressure, respectively. Using the sensor-driven approach, I can assure my project acquires precise and real-time data collection, which enables a detailed examination of aerodynamic phenomena with suitable weather conditions, given no reliance on digital simulations.

Data analysis, also becomes another critical component in this research, with the collected measurements processed and visualized through graphs to facilitate comparison across different shape configurations. Certain key metrics can be found in the graphs represented in Chapter 4, such as newtons for force, cubic meters per second for airflow and kilopascals for pressure. The analysis tends to focus on empirical data, therefore this study can validate theoretical aerodynamic principles and provide practical insights into how subtle geometric changes can yield significant performance improvements.

Throughout this project, a representation is found of the knowledge and skills acquired on my academic journey, drawing on multiple disciplines within the degree program. This process breaks down into understanding the design of each shape,

coding for programming and calibrating the sensor to electronic connectivity for integration of the sensors with the data acquisition system. Generally, this hands-on process reinforces technical proficiency and also navigates challenges with critical thinking, such as data noise and environmental variables.

2 Literature Review

Throughout this chapter of the thesis, a literature review is provided based on background research, regarding my study in testing and gathering airflow measurements with various different shapes, 3D printed on top of a small moving vehicle. In Section 2.1, a thorough investigation in understanding the principles of air friction can be found. Through Section 2.2, the fluid dynamics are focused with important mathematical foundations being researched and analysed to provide fundamental viewpoints in further analysis, and a theoretical overview of how certain fluid mechanics are important in testing the vehicle's aerodynamics. In Section 2.3, the sensors used in this research are studied to understand the key metrics each one captures, in order to obtain data to view and compare for my research goal. Through Section 2.4, certain environmental factors are considered to ensure the data gathered can be reliable and valid when comparing different sensor outputs. Lastly, in both Sections 2.5 and 2.6, a study in the selection of particulate incline angles is thoroughly analysed, whilst understanding how flow trajectories are affected in motion using the Bernoulli's equation.

2.1 Air Friction

The resistive force experienced by an object is due to the momentum transfer from air molecules colliding with and flowing around it. The flow resistance of air around a vehicle is related to what shape the object is and what degree of surface smoothness it is [1].

$$\mathbf{F} = \mathbf{k}\mathbf{v}^2 = \frac{1}{2}\mathbf{C}\rho\mathbf{A}\mathbf{v}^2$$

The equation above determines that drag force is proportional to the square of the velocity, which equates to drag increasing drastically when speed goes up.

2.2 Fluid Dynamics

This section will focus on the literature regarding fluid dynamics, a crucial role for this thesis research in gathering analytical data in the movement of fluids and the forces acting on them. The interaction between air and solid bodies in motion are variables with fundamental principles being reviewed to understand the context of this research, while also ensuring the importance in the aerodynamics of numerous vehicles with how its application in this study works regarding the measurement of airflow.

2.2.1 Mathematical Foundations

Previous studies have shown that the equations governing fluid dynamics are the main foundations which root in the laws fundamentally found in physics, specifically in conservation of mass [2], momentum [3] and energy [4]. These equations, regarding the laws described above for both liquids and gases in their behaviour in motion, are critical for predicting aerodynamic phenomena. Moreover, it is essential to grasp

these equations to accurately model fluid flows, particularly in high-performance applications. Therefore, applications such that can be used in vehicle design to ensure that there are no small inaccuracies in predictions and to avoid significant consequences [5]. The following methods discrete the continuous equations into a solvable format.

1. Continuity Equation - Conservation of Mass:

   Fundamentally, the equation which stems from the law of conservation of mass is the continuity equation. In any given volume of fluid, the amount of mass cannot change unless there is an inflow or outflow of mass, resulting the mass of the fluid being conserved across the entire domain, with mass incapable to be destroyed or created [6].

   For an incompressible flow, where fluid density remains constant, a simplified continuity equation is shown:

$$\frac{\partial u}{\partial x} + \frac{\partial v}{\partial y} + \frac{\partial w}{\partial z} = 0$$

   The above equation represents **u**, **v**, and **w** as velocity components, whereas **x**, **y**, and **z** represent directions, respectively. The divergence of the velocity field is zero, which indicates that implying any contraction in one direction must be balanced by an expansion in another direction to maintain a constant volume.

   For a compressible flow, where fluid density can change, a general form of the continuity equation is shown:

$$\frac{\partial \rho}{\partial t} + \nabla \cdot (\rho \mathbf{u}) = 0$$

Using this general form equation, with ρ representing fluid density and $\mathbf{u}$ representing the velocity sector, variations in density can be accounted for. Once the calculation is successful, the result becomes applicable to a broader range of fluid dynamic issues.

2. Momentum Navier-Stokes Equation

   Understanding the Navier-Stokes equations is key to describe the conservation of momentum in a fluid. The equation is derived from Newton's second law, which states that the rate of change of momentum in a fluid element is equal to the sum of the forces acting on it. Under various conditions, these equations can provide a detailed description of how fluids move, resulting in being most widely used [7].

   In vector form, the Navier-Stokes equation for the incompressible fluid is written as:

$$\rho(\frac{\partial u}{\partial t} + \mathbf{u} \cdot \nabla \mathbf{u}) = -\nabla \mathbf{p} + \mu \nabla^2 \mathbf{u} + \mathbf{f}$$

   To understand the equation above in how it is formed, the ρ is represented as the fluid density, $\mathbf{u}$ as the velocity vector, $\mathbf{p}$ as the pressure, μ as the dynamic viscosity, and $\mathbf{f}$ as the external forces including gravitational or electromagnetic. The equation consists of convective and local acceleration terms, which constitute the change in velocity over time and space, which equal to the pressure gradient, viscous forces, and external body forces. In the context of aerodynamics, the pressure ∇p is the driving force for fluid motion, where pressure differences dictate lift and drag forces around a body.

3. Conservation of Energy Equation:

Derived from the first law of thermodynamics [8], the equation can only be converted from one form to another and it cannot be created or destroyed. Such energies can exist in fluid dynamics with forms such as kinetic energy, potential energy and internal energy.

The compressible flow in the energy equation is such:

$$\frac{\partial(\rho e)}{\partial t} + \nabla \cdot (\rho e \mathbf{u}) = -\nabla \cdot \mathbf{q} + \mathbf{f} \cdot \mathbf{u} + \mathbf{\Phi}$$

Looking at the above calculation [8], $\mathbf{e}$ is the total energy per unit mass, $\mathbf{q}$ is the heat flux vector, and $\mathbf{\Phi}$ is the viscous dissipation function. The rate of change of energy in a fluid element is equal to the work done by external forces, viscous effects and heat transfer through conduction. It is important to see that in high-speed aerodynamics where temperature and pressure variations play significant roles, the energy equations are crucial in simulations involving compressible flows.

Using the above governing equations in fluid dynamics, a graphical output from practical testing analysis can be formed. The foundation for predicting complex fluid behavior can describe how mass, momentum and energy are concerned within fluid. Critical real-world aerodynamic problems can be solved by understanding these equations and their physical significance accurately and efficiently.

2.3 Sensor Functionality in Aerodynamics

Appropriate sensors are used to analyse the aerodynamic performance, resulting in capturing data in flow, pressure and force. This section discusses the principles of the

selected sensors, their functionality, and their role in gathering precise measurements for this research.

2.3.1 Flow Sensor

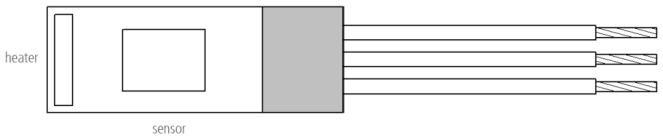

Figure 2.1: Flow Sensor [9]

The flow sensors, as it is illustrated in Figure 2.1, which are selected for this research is the FS7 [9], which can precisely provide airflow measurements that can be used to understand the aerodynamic flow around an object depending on its placement. The operation of the sensor is based on thermal anemometry, utilizing a temperature sensor and a heated element to measure the cooling effect caused by airflow. [10] When this principle is used, accurate detection of flow rate variations can be studied to make suitable real-time aerodynamic assessments.

The chosen sensor for this research uses three primary output connections: a heater, a temperature sensor, and a ground. All three of these output connections provide important factors in gathering data from airflow passing over its surface, with the heater element introducing a control amount of heat and the temperature sensor detecting changes in heat dissipation caused by airflow. The aim of using this particular sensor is to be able to understand its airflow patterns, in order to be able to optimise sensor placement and aerodynamic design.

2.3.2 Pressure Sensor

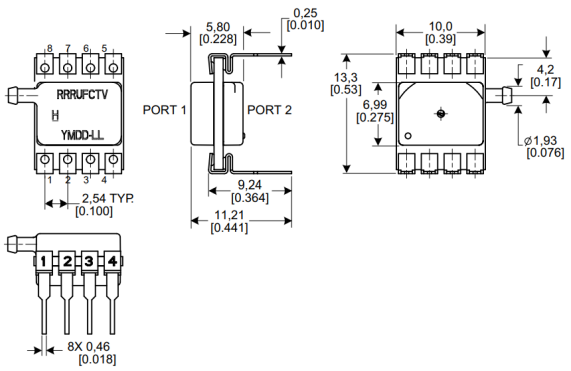

Figure 2.2: Pressure Sensor [11]

The pressure sensors selected for this research is the board mount pressure sensor DIP RN [11] as shown in Figure 2.2, which provides a high-resolution digital output with an ability to measure low-pressure differentials. This sensor operates based on piezoresistive technology [12], where a diaphragm is silicon-based and it deforms based on response to pressure variations. An alteration in the resistance of the internal sensing elements regarding the deformation occurs, outputting a digital output through an integrated signal-conditioning circuit.

The chosen sensor is able to provide I^2C digital communication, allowing direct integration with the Jetson Nano for real-time pressure data acquisition, and it is designed for applications requiring low power consumption and high stability. A characterization of the aerodynamic flow under varying environmental conditions and terrain, helps to measure static and dynamic pressure changes around an object. By analysing this data, it becomes possible to optimise sensor placements and access the impact of wind resistance, thus refining aerodynamic efficiency. The vehicle's design is not really affected from its size, as it enables the possibility for the sensor to be positioned in critical locations.

2.3.3 Load Cell Sensor

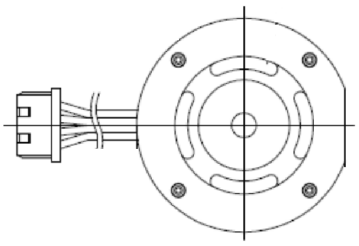

Figure 2.3: Load Cell Sensor [13]

The load cell sensor selected for this research is the FX1901 as shown in Figure 2.3, which is capable to measure force and load variations [13]. The strain gauge principle is used for the operation of this sensor, where internal resistive elements deform under applied force, causing a change in electrical resistance. Therefore, it converts into an analog voltage signal, which can be processed to determine the applied force.

A measurement of down force and weight distribution takes place to analyse the data given when the vehicle shifts under different terrains and inclines, which can affect traction and stability. Certain external aerodynamic forces can be identified using this sensor that provides a possibility of detecting subtle variations in applied force.

2.4 Environmental Factors

Outlying conditions are important to take into account in order to ensure the data can be compared in equal terms. Factors in weather conditions, effects and other external conditions are assessed below to take into consideration while gathering the different values with the different shapes.

2.4.1 Meteorological

Meteorological conditions are important to consider, especially when it comes to the current temperature when conducting the testing outdoors. The graph above illustrates a founding which was administered by Vilamajo, a researcher in aerodynamics, exploring the variation in air density with different temperature conditions [14].

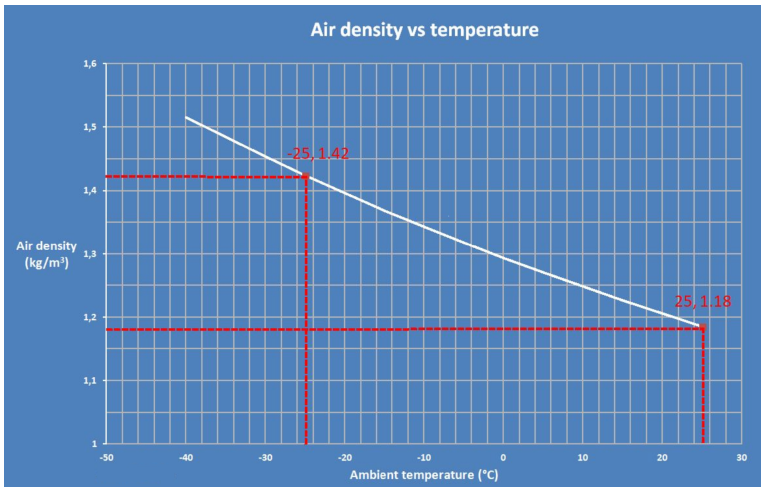

Figure 2.4: Variation of air density with different temperature recordings [14]

When gathering data as shown in Figure 2.4, the air density can vary due to minor differences in the temperature, humidity and air pressure. When considering the ideal gas law [15], as temperature increases, the air density decreases which results to reduced lift, drag and pressure forces. Humidity also has certain affects

due to water vapour being less dense than dry air [16] with aerodynamic forces being decreased. Minor differences in temperature such as 1 to 2 ° C or humidity such as 5 to 10 % would not make huge differences to justify accuracy. Considering a difference in air pressure, when it becomes lower, flow separation effects might shift [17] and certain differences would provide drastic different data. High temperature, humidity differences and air pressure variations can affect findings in both the flow and load cell sensors, resulting in inaccurate data when comparing different test results.

Wind is another important factor that can alter force and pressure readings, resulting in an increase in dynamic pressure and thus adjusting the wind speed. Asymmetry can also be found especially considering the wind direction, with data showing altered pressure distributions and force vectors [18]. To ensure comparable data, calm air should be an environmental condition that is a must for valid findings.

2.4.2 Particulate Effects

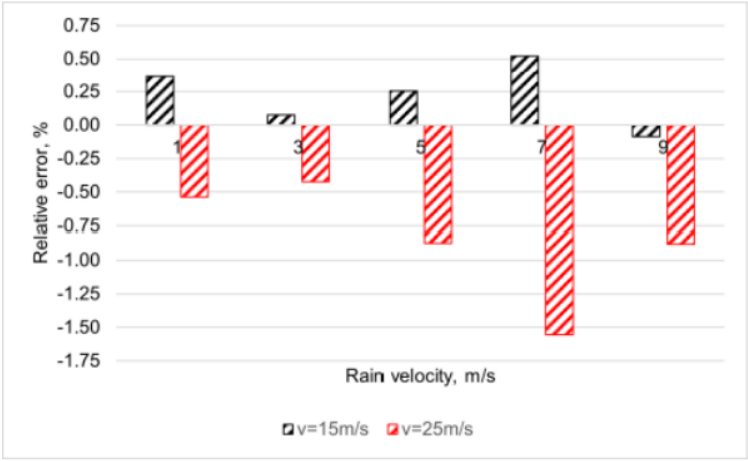

Figure 2.5: Error distribution of the drag force vair=0 m/s case [19]

Similar and good weather conditions when conducting the testing phase is important in aerodynamics, to ensure data comparison is valid and the shape comparisons

are accurate. A research conducted by Lakatos and Brúnó shows error margins when the rainy conditions are taking place, which can be reflected from Figure 2.5, which impact the data accuracy [19].

Certain physical effects are important to understand when it comes to getting accurate results upon conducting the testing phase. Environmental particles such as dust, debris or precipitation can influence the aerodynamic data and sensor measurements gathered. The particles mentioned above can contribute to an increase of surface roughness, which results in aerodynamic loss through its interaction with the boundary layer [20]. A flow disruption can be occurred when particles in the air or water droplets alter local airflow patterns, affecting pressure distributions around the shape tested. In rainy conditions, accumulated water can alternate the weight, resulting in data not being treated equally when conducting the experiment.

2.4.3 External Interference

When conducting the testing phase, certain external interference is important to be aware of, for more accurate findings. Vibrations or turbulence can cause the data to be twisted, due to a lack of a good suspension or windy conditions. This should be checked and observed to ensure the data gathered is accurate and can be compared when testing different shapes.

It seems reasonable that when conducting the testing phase, vehicle vibrations will occur of some sorts due to a slight surface difference when the vehicle moves from location A to location B. Vibrations do contribute to intermediate frequencies in radar signals, which reduce the signal-to-noise ratio, resulting in lowering probability and accuracy of target detection [21]. The reference also confirms providing graphs, that roadway texture is a factor that is bound to provide some sort of vibration, which might slightly alter the data.

Turbulence is bound to occur, specifically in rough windy conditions. Flow sensors due to wind gusts would produce inaccurate findings and the data gathered cannot be used during analysis. Certain experiments that were found in a reference conclude in confirming that certain aerodynamic turbulence, from vehicle motion or environmental winds, amplify sensor noise, especially when it is combined with vibrations [21].

2.5 Angular Measurements in Aerodynamics

Performance metrics are a critical topic when it comes to vehicle design and engineering, with the front incline angle and rear slope angle playing a pivotal role. Usually, the inclination angles of a vehicles body comes from the suspensions kinematics and stiffness that are smaller if the vehicle is equipped with dependent suspensions [22].

These principles are mostly governed by Bernoulli's equation [23]:

$$p + \frac{1}{2}\rho v^2 + \rho g h = \text{constant}$$

p represents static pressure, ρ is the fluid density, **v** is the flow velocity, **g** is the gravitational acceleration and **h** is the elevation height.

Where this equation represents the understanding of the theoretical effects of front incline angles, real-world vehicle examples can be used on why each angle as shown in Figure 2.6 is appropriate for each vehicle model.

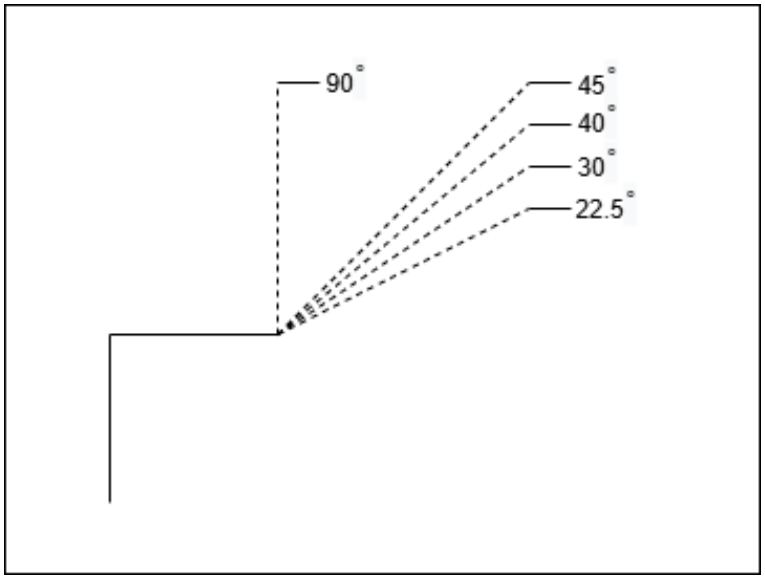

Figure 2.6: Incline angles

Front Incline Angle of 22.5°:

This angle is used for minimizing the projected frontal area, reducing both air stagnation and drag with air flowing smoothly over the vehicle maintaining high velocity and low pressure per Bernoulli's equation. Applying this incline, the positive effect is battery or fuel efficiency, due to airflow velocity over the top which reduces pressure [23], with speed increasing but traction reducing.

Front Incline Angle of 30°:

Pressure and drag increases slightly using this angle, and it becomes more appropriate when aiming for front-end stability. Grip is enhanced and allows high velocity per Bernoulli's equation. Mixed driving conditions are probably most suited, using this angle with a compromise between speed and cornering stability. Through aggressive turns, it might still compromise traction with moderate lift.

Front Incline Angle of 40°:

This angle introduces turbulence over the top, potentially initiating downforce, with front-end grip enhanced. Stability in corners is improved, with aggressive

handling making driving suitable. When compared with lower angles, speed and efficiency is reduced, resulting with drag penalised.

Front Incline Angle of 45°:

With this particular angle becoming the middle point between 0 and 90, downforce is promoted and lift is reduced, with traction being greatly enhanced. In high grip scenarios, this angle becomes the best choice when the vehicle is in corners requiring stability. Power is required more if the aim of the vehicle is requiring performance.

Front Incline Angle of 90°:

Largest possible frontal area is found using this angle with highest drag and pressure measured naturally when considering using this angle in the equation. Downforce is generated, with grip improved, due to airflow becoming highly turbulent. The highest drag is enforced due to this angular incline, with the reduction of speed and efficiency being key.

2.6 Flow Trajectories

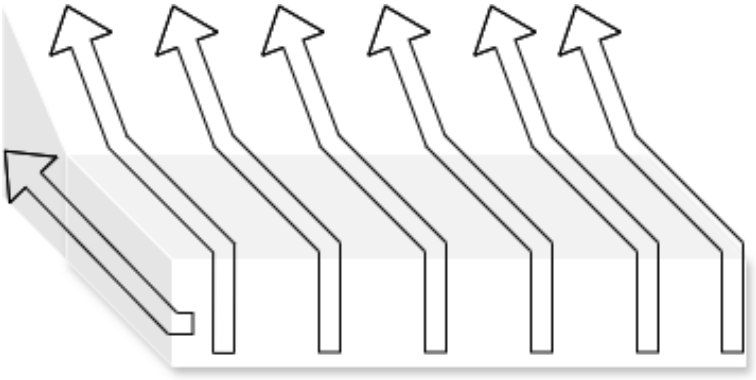

Figure 2.7: Airflow Trajectories in Front of a Vehicle

Velocity tends to flow as shown in Figure 2.7 over the vehicle body, with stream

line flows being disorganised for the shape of the vehicle [24]. While the stream line passes perfectly without any obstacles blocking the airflow, the velocity of the car will increase. The air in the path of its flow gets less resistance, with each specific spot of the vehicle providing different measurements, hence certain sensors placed correctly in environmental testing is needed.

3 Methodology

This chapter delineates the comprehensive methodology employed to prepare and execute the experimental testing integral to this research. All necessary components and how they were all connected within the rolly vehicle is described, and the specific type of remote vehicle utilized. The preparatory phase encompassed multiple facets, including the fabrication and design of different top-mounted test shapes via 3D printing, which were affixed to the RC vehicle for aerodynamic evaluation.

The RC vehicle employed in this study was utilized in another research conducted by Malik [25]. Malik's expertise was really valuable and instrumental in facilitating various preparatory activities, with their report providing critical insights into the vehicle's existing components, all of which are detailed below in this chapter. A thorough understanding of the usage of all components allowed me to input correct sensors that can work with the current schematic, ensuring operational efficacy.

All 3D printed shapes were designed and conceptualized by the author, however, Malik's proficiency in 3D modelling significantly enhanced the design process, resulting in precise geometries required for testing. This chapter further describes the appearance of these shapes and the strategic placement of sensors within them. Geometric differences which influence aerodynamic performance is crucial to understand, in order to achieve my research objective, hence the positioning of these sensors across all shapes.

Additionally, an outline of the complete testing procedure, from data visualiza-

tion to track mapping, is discussed and analysed. This provides a practical framework which underpins this thesis, laying out a comprehensive overview. Real-time data acquired from all sensors were graphically represented, with all systematically findings compared and analysed in Chapter 4.

3.1 Experimental Platform and Instrumentation

This section mentions the hardware essential to achieve the objectives of my research. A detailed description of the remote controlled vehicle with its necessary specifications, a schematic without sensor placement, and all components required to enable the sensors to collect and output visualized data. Subsequent modifications were made to adapt the vehicle to meet the specific requirements of this study.

3.1.1 RC Vehicle

Figure 3.1: Reely Stagger Rover (left) and Flysky Remote Controller(right)

The vehicle used for this experiment is a small Reely Stagger Rover as shown in Figure 3.1 scaled at 1:10, which can be referred to the size of other model cars. This vehicle has been chosen due to its reliable acceleration and speeds up to 45km/h, therefore satisfying needs that would output measurements for my testing. It is

powered by a 7.4V 3500 mAh battery, which can be lasting enough to power necessary components. It is controlled with a Flysky-16 remote controller that also has a FSiA6B receiver that offers decent responsiveness. [25]

3.1.2 Integrated Microcontroller and Multiplexing Systems

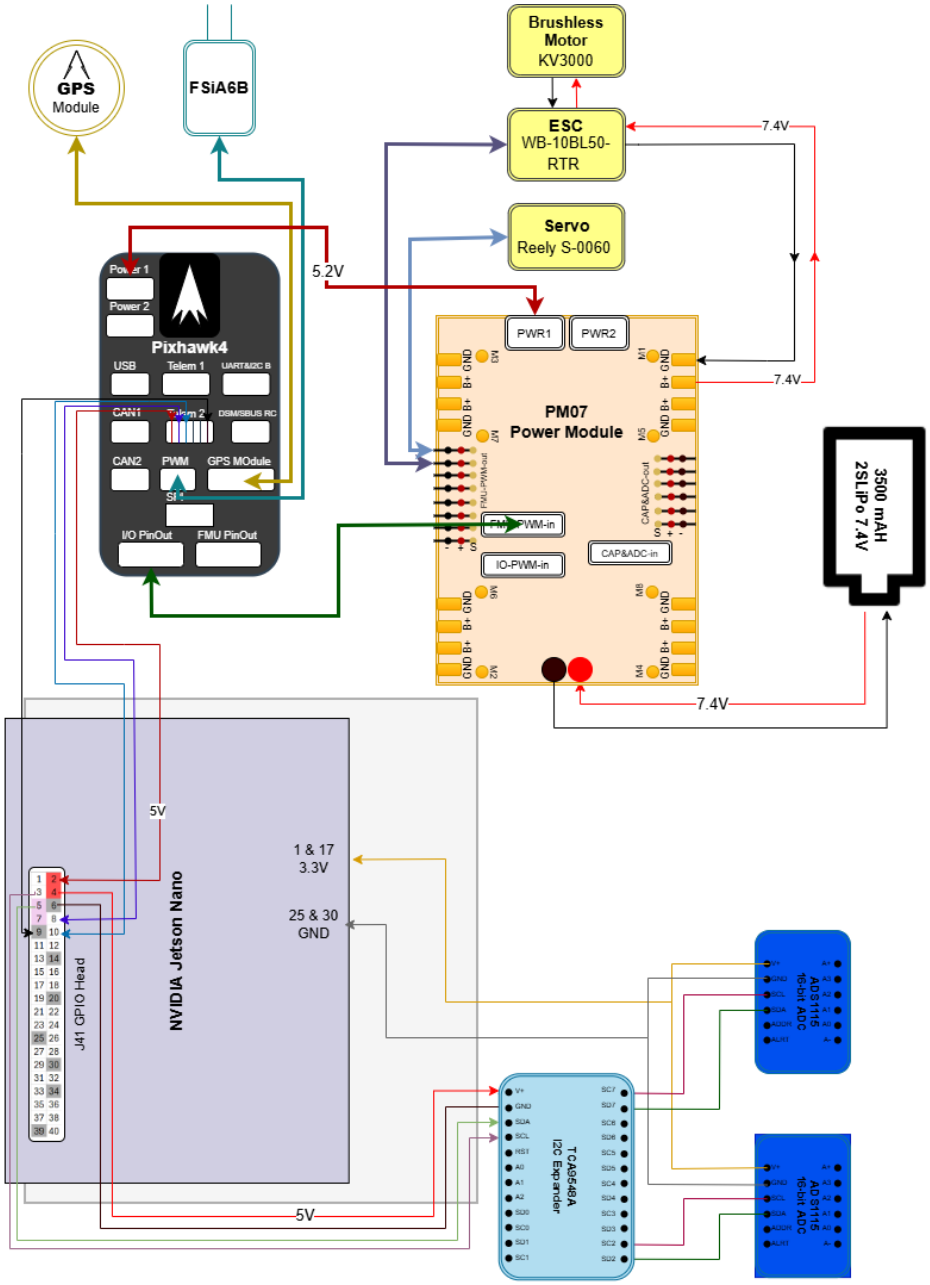

Figure 3.2: Schematic of components

In Figure 3.2, the schematic shows all components used in the vehicle except the sensors. A battery with 7.4V and a capacity of 3500mAH powers the PM07, which itself provides correct voltage measures to the Pixhawk4 and other important motors for the vehicle to be able to function. The power module has a crucial connection to the Pixhawk4 with a regulated 5.2V of power, monitoring battery voltage and current. A 6-pin JST-GH cable links the PM07's power output port PWR1 to one of the Pixhawk 4's power ports Power 1, transmitting analog voltage and current signals for battery monitoring. The Pixhawk4 is also connected with the GPS module and the FSiA6B for manual control with the remote controller.

The connection between the NVIDIA Jetson Nano and the Pixhawk 4 is crucial to enable communication for autonomous vehicle applications. Using a 6-pin JST-GH connector, the PixHawk 4's TELEM2 port is wired to the Jetson Nano's UART pins to transmit MAVLink messages, allowing the Nano to read sensor data and send control commands. The Jetson Nano, acting as a companion computer, processes computationally intensive tasks and the Pixhawk 4 handles real-time control.

The I2C multiplexer connects with the Jetson Nano with the aim of managing multiple I2C devices, such as the ADS1115. The Jetson Nano's I2C pins are connected to the multiplexer's main SDA and SCL pins using jumper wires, enabling communication at its default I2C address 0x70. Ensuring compatible logic levels, the TCA9548A's power and ground are connected to the Jetson Nano's 3.3V and GND pins, respectively. This setup allows the Jetson Nano to selectively route I2C signals to one of the eight channels the Multiplexer possesses, facilitating scalable sensor integration for data acquisition.

The TCA9548A I2C Multiplexer connects to both the ADS1115 analog to digital converter through one of its eight I2C channels. One of the ADS1115s SDA and SCL pins are wired to the TCA9548A's SD2 and SC2 pins, respectively, which enables I2C communication at the ADS1115's default address. Similarly, the second ADS1115s

is also connected to the SD7 and SC7, achieving the same goal. Both the ADS1115s are used for wire flexibility and are connected to a 3.3V and ground pins, which can be found in the Jetson Nano, ensuring operational compatibility. Using the I2C multiplexer and both ADS1115s is necessary to achieve the possibility of handling 10 different sensors gathering data simultaneously, which enables a high-precision analog-to-digital conversion for all sensors. In Section 3.2 a detailed connection between the I2C multiplexer, ADS1115s and sensors can be found.

This section focuses on each component which is found in the above schematic, but with detail on its functionality. All components were necessary to achieve the aim of this research, ensuring data gathering of five flow sensors, two pressure sensors and the force load cell sensor.

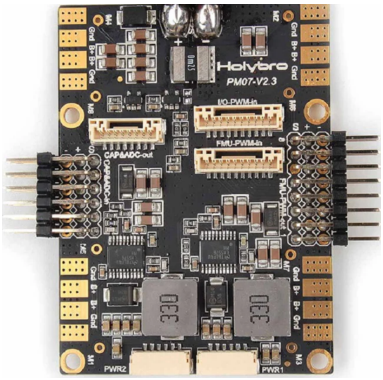

Figure 3.3: Power Management Board

The PM07 is a power management board as shown in Figure 3.3 that is used to regulate and distribute power to various components. It takes input from a battery such as a 7.4V and regulates it to provide stable voltage outputs of 5V or 3.3V, which can satisfy when powering the sensors.

Figure 3.4: Open-Source Autopilot System

The Holybro Pixhawk 4 as shown in Figure 3.4, is an open-source autopilot system, which integrates hardware and software to control a vehicle's movement, process sensor inputs, and execute autonomous or semi-autonomous tasks. It provides the possibility to support a wide range of sensors through an interface such as a I2C, which collects and processes various sensor data in real-time, allowing to log measurements taken.

Figure 3.5: GNSS module

The PX4 GPS module as shown in Figure 3.5, is a global navigation satellite system that becomes another key component in providing precise location, velocity and time data. The importance of this module in this research is for real-time data to be seen, such as position and speed, to map the data and compare when having

different shapes on top.

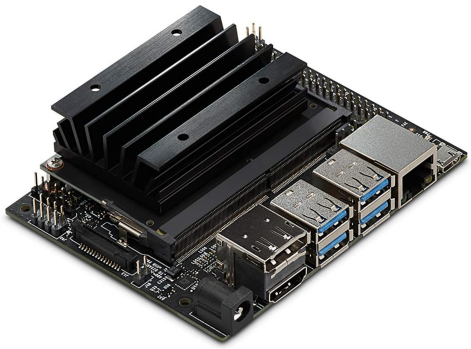

Figure 3.6: Jetson Nano - Single-Board Computer

The most significant component which ensures the data processing runs smoothly is the Jetson Nano as shown in Figure 3.6, a single-board computer that is able to run large volumes of data. It allows the possibility to process and visualize the sensor data with scripts, and allows findings, such as graphs, to be used to compare various data.

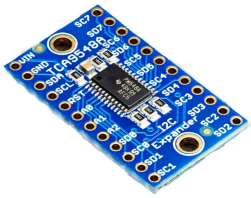

Figure 3.7: I2C Multiplexer

Communication is managed using the I2C multiplexer as shown in Figure 3.7, between the microcontroller and multiple I2C devices, allowing similar sensors to be inputted around the vehicle. Many sensors have fixed or limited configurable addresses, causing conflicts if multiple identical sensors are used. It creates multiple I2C sub-buses, each acting as an independent I2C bus, which allows to connect more devices than a single bus could handle.

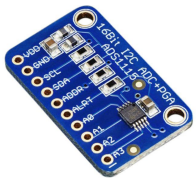

Figure 3.8: ADS1115 16-bit ADC

The ADS1115 as shown in Figure 3.8 is a 16-bit analog-to-digital converter, utilized in this research to acquire high-precision sensor data. It features four single-ended or two differential analog input channels, enabling accurate measurement of sensor outputs. The gathered data acquisition ensures that the analog signals from the sensors mounted on 3D-printed test shapes translate to digital data, which is subsequently visualized to analyse aerodynamic performance.

3.2 Sensor Placement and Connectivity

The precise placement and connection of all sensors, comprising five flow sensors, two pressure sensors and one force load cell sensor, are important to achieve accurate and reliable data acquisition. The position assigned for each sensor is strategically placed to capture essential system parameters that are interfaced with three ADS1115 16-bit analog-to-digital converters. All three are connected with the Jetson Nano micro-controller, but two are connected through the TCA9548A I2C multiplexer, due to the Jetson Nano having an availability of only two SDA/SCL ports. All components operate on a 2.2V power supply with a common ground to ensure electrical reference levels.

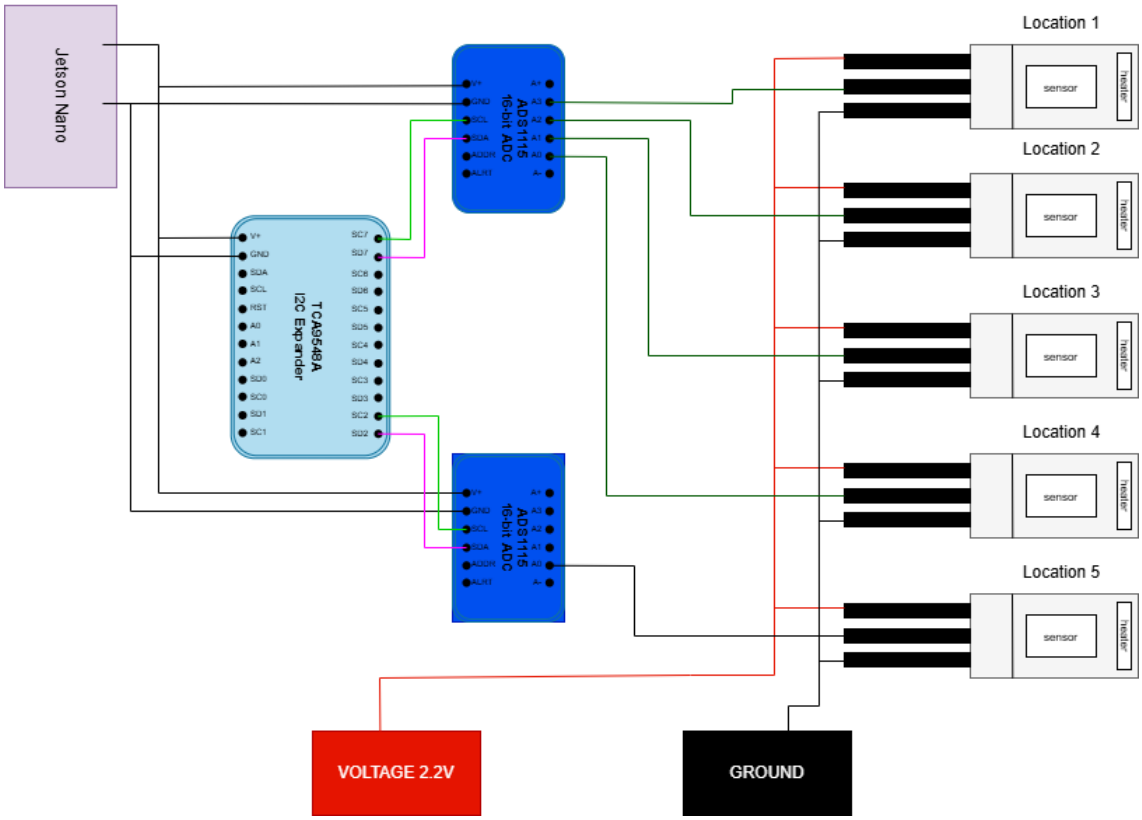

Figure 3.9: Schematic of Flow Sensors

The schematic in Figure 3.9 displays the wiring of the five flow sensors to the other components. With only 4 of the flow sensors connected to the ADS1115, due to insufficient space, one of them is directly linked to the second ADS1115. Electrically, the four analog flow sensors are connected to the first ADS1115's analog input channels A0 to A3 and the fifth is connected to the A0 analog input channel in the second ADS1115. Both ADS1115s are linked to the TCA9548A I2C multiplexer channels of SD2/SC2 and SD7/SC7 respectively, which therefore is connected to the Jetson Nano. All flow sensors are powered with a 3.3V supply and their respective ground pin is connected to the system ground.

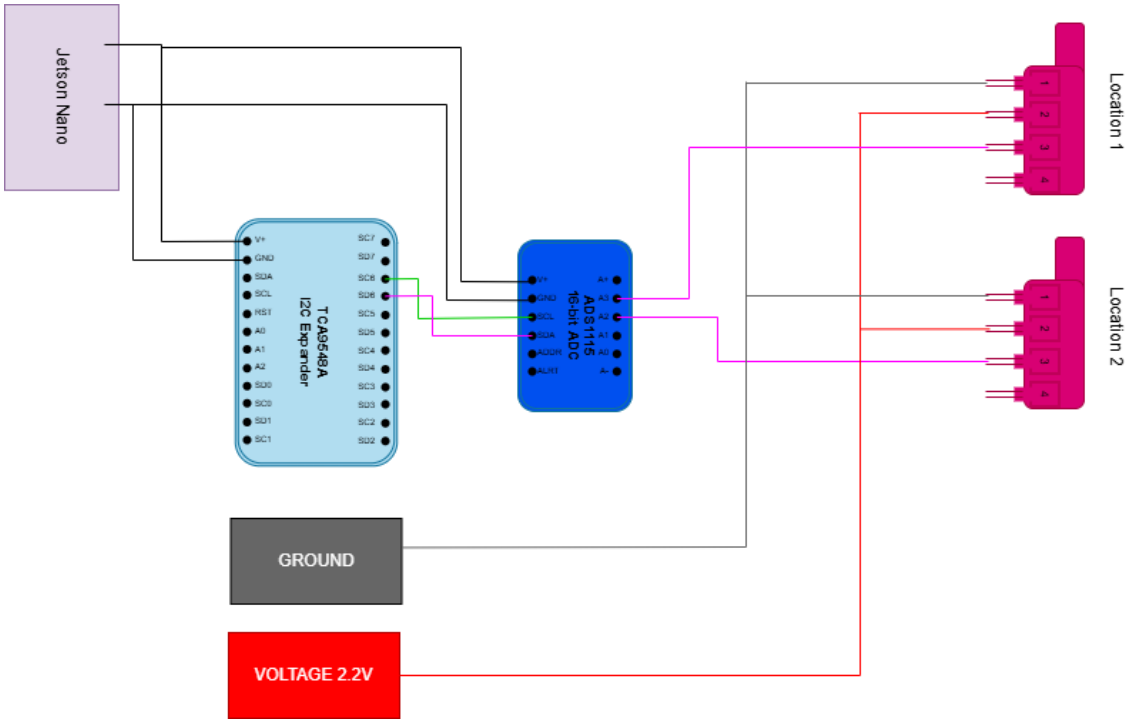

Figure 3.10: Schematic of Pressure Sensors

Figure 3.10 focuses on the wiring of the pressure sensors to gather appropriate data. The two pressure sensors do fit to be connected to a single ADS1115, which furthermore joined to a TCA9548A Channel SD6/SC6. Pin 4 on each pressure sensor tends to be used for calibration, but while testing, it does not become necessary to connect. Both pressure sensors, similarly to the flow sensors, are powered with a 3.3V supply each and with their respective ground pin connected to a common system ground.

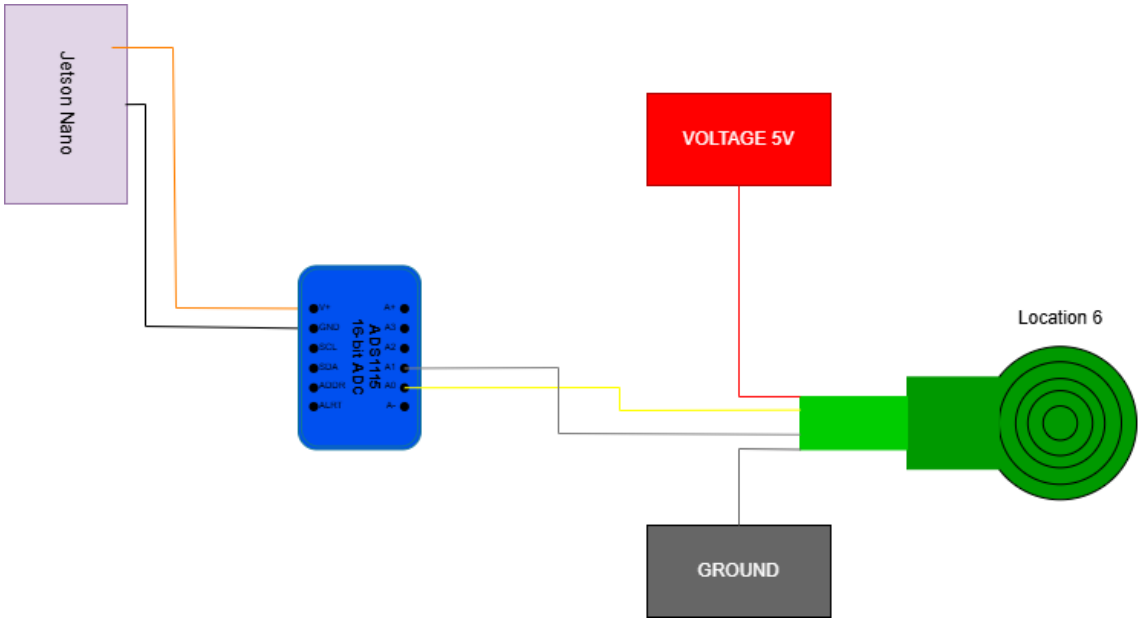

Figure 3.11: Schematic of Force Sensor

From the force sensor shown in Figure 3.11, it similarly connects directly to the ADS1115 converter, such as the flow sensor. Both SDA/SCL are connected to the A0/A1 respectively, the voltage is connected to a 5V power supply and the ground is connected to a common system ground.

	Location 1	**Location 2**	**Location 3**	**Location 4**	**Location 5**	**Location 6**
Flow Sensor	✓	✓	✓	✓	✓	-
Pressure Sensor	✓	-	-	-	✓	-
Load Cell Sensor	-	-	-	-	-	✓

Table 3.1: Sensor placement in each location

The sensor system, which is designed to evaluate aerodynamic and structural impacts of various vehicle cover shapes, consists of five flow sensors, two pressure sensors and one force load cell sensor, placed at six distinct locations on the vehicle as shown in Table 3.1. The six locations on the vehicle are on the front, the right side, the left side, the top, the back and on the front bumper. These positions are critical for capturing data on fluid dynamics and mechanical forces influenced by different cover shapes.

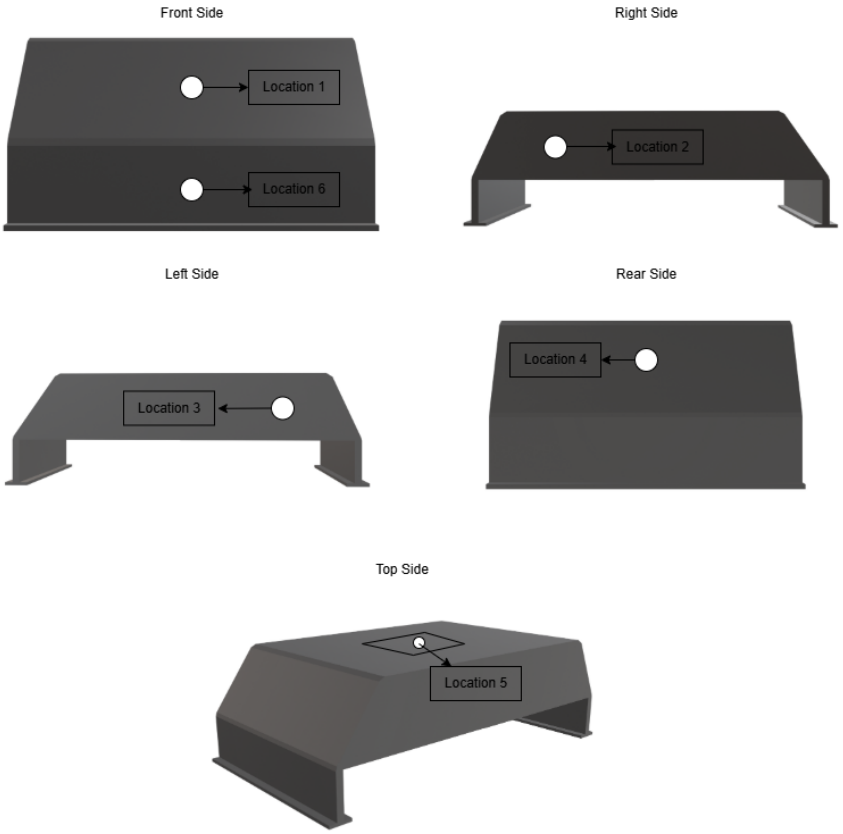

Figure 3.12: Every location of each sensor on all sides on the cover of the vehicle

Figure 3.12 showcases all sides of one of the shapes printed, which is used during the testing phase, importantly understanding where each sensor was placed to gather data necessary for this project. Similarly, all other shapes had similar positions on where each sensor was placed. The front of the vehicle which is in Location 1 hosts a flow sensor and a pressure sensor, positioned to capture critical aerodynamic data where the vehicle first encounters oncoming airflow. This specific location is pivotal due to the highest initial air impact, making it essential for measuring airflow velocity and pressure. Specifically, this location will show important data of how different shape variations impact pressure distribution and potential turbulence, while also seeing different data on frontal drag. Similarly in Location 5, there is a flow sensor and a pressure sensor, which is in the top side of the vehicle. The logic behind this placement is to analyse and monitor airflow and pressure over the upper surface. The top area also becomes crucial to analyse, due to the difference in air streamlines over the vehicle.

In the right and left side of the vehicle, we can find Location 2 and 3, respectively. Both of each of these locations also have one flow sensor, which are both important to analyse how the airflow reacts on both sides when the vehicle is turning right and left. In Location 4, only one flow sensor is placed to see what airflow goes through the rear end of the vehicle. This location becomes significant as the airflow separates, forming wake patterns that contribute to drag and affect vehicle stability. Location 6, which is located in the front bumper, has the only one force load cell sensor. The data from this sensor will show data of how much mechanical stress the vehicle indulges from airflow impact and road-induced forces.

3.3 3D-Printed Shape Models

	Shape 1	**Shape 2**	**Shape 3**	**Shape 4**	**Shape 5**
Front Angle	45°	22.5°	30°	40°	90°
Rear Angle	60°	22.5°	90°	60°	90°

Table 3.2: Angles in all shapes

To understand and investigate the varying aerodynamic effects on different roof geometries, five different shapes were designed and printed using a 3D-printer. Each shape is characterised by unique angular profiles to represent a spectrum of vehicle configurations. With the help of Malik in designing the following shapes, they were engineered to differ primarily in the inclination angles of their leading, trailing, and lateral surfaces, thereby influencing airflow and pressure distribution. In Table 3.2, all shapes with their respective angles in both rear and front can be seen for comparison.

Figure 3.13: Shape with frontal 45° and slope of 60°

This shape in Figure 3.13, is designed to mimic traditional SUV profiles, with a leading edge inclination of 45° and a slopping trail of 60°. These specific angles will aim to promote early flow separation at the trailing edge.

Figure 3.14: Shape with both frontal and slope of 22.5°

With a symmetrical profile, this shape in Figure 3.14, has a front and rear angle of 22.5°. Its design aims to minimise drag and maintain smooth airflow.

Figure 3.15: Shape with frontal 30° and slope of 90°

With a front angle of 30° and a rear angle of 90°, this shape in Figure 3.15, aims to enhance downforce but increase drag, due to abrupt flow detachment.

Figure 3.16: Shape with frontal 40° and slope of 60°

Having a leading edge of 40° and a slopping trail of 60°, similar with the first shape, it has a slight difference with its front angle, mainly designed to see the variety in data between those two, even in small angle differences as shown in Figure 3.16.

Figure 3.17: Shape with both frontal and slope of 90°

With a front and rear angle of 90°, this box shaped design shown in Figure 3.17 aims to maximise flow separation and drag. With the air flow being directly hit in the frontal part, a huge variety of data comparing with the other shapes in both the flow sensors and pressure sensors is expected to be found.

3.4 Testing Procedure

The testing procedure was carefully developed to produce accurate and repeatable aerodynamic data for analysis. The five distinct 3D-printed shapes were interchangeably mounted onto the base of the RC vehicle, with a slide-in mechanism, which was considered when matched with the base of the vehicle, to ensure each shape was consistently positioned and securely fastened. To prevent any bias regarding the sequence of the testing, the shapes were switched in a randomised order, with the attachment process streamlined to minimise setup time between trials. All sensors were connected in the beginning accordingly to their position, with each shape containing holes for placement of where they should be, respectively. Temperature consistency was a key priority for data validation, as fluctuations could alter air properties like density and viscosity, with results being skewed. Each model was cleaned, with dust and any debris removed to ensure clear data validation and to remove any disruptions to airflow.

To validate the data collected from the pressure and flow sensors, a distinct track simulation was integrated, which is discussed further in section 3.4.1. This diverse

track was critical for validating the findings, as it allowed thorough examination of how the shapes performed beyond a single scenario, providing a more robust dataset. These measures collectively ensured the experimental conditions remained controlled and the data was reliable.

3.4.1 Test Track Setup

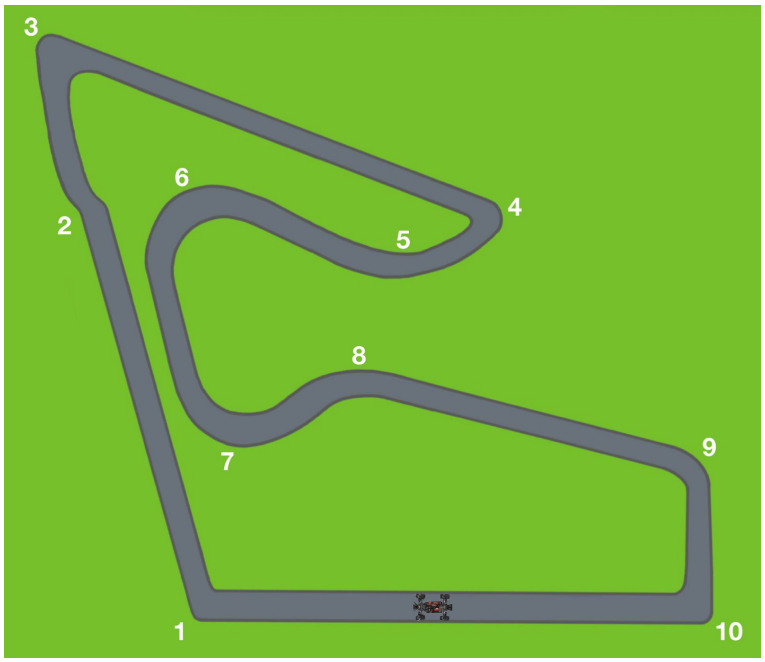

Figure 3.18: Tracks used for testing

The main testing track, which can be found in Figure 3.18, is inspired from the Spielberg track in Austria [26]. The layout became a good idea to use due to how diverse it is of straights and turns, which results in gathering the data needed to see from all flow, pressure and force sensors. Due to a limited constrained environment space, the track has been scaled down to 1:10 from its original 4.318 km length to about 431.8 m of circuit. The many straights and different types of turns can output a good chunk of data from all sensors in different situations. Due to the different incline angles used, each turn is unique on what would be the best alternative with each angle, in viewing what is the best speed, stability, and efficiency.

Each turn has a specific data point set which would be interesting to see after having the results all together. The first turn is a tight right turn, which would be critical to examine the right and left flow sensors at all incline angles. In turn 2, it becomes a slight small left bend which tends for the data in the front and back, becoming the most crucial one. In both turn 3 and turn 4, it becomes another interesting check when assessing all sensors. From turn 5 to turn 8, the track changes direction from right to left to right and the side sensors would produce opposite data, assuming that the vehicle goes at a stable speed, and would show different numbers across that section. Towards the end of the track, both turn 9 and turn 10, become full throttle high-speed turns that would highly affect the lower angle incline in speed and downforce for the higher angles.

3.4.2 Sensor Calibration

Sensor calibration is a vital process to ensure accuracy upon data been collected from all sensors. When the vehicle is stationary, the sensors are calibrated accordingly, resulting the data being zero for all measurement units, respectively. It is important to establish a baseline using this zero reading, indicating there is no force, airflow or pressure changes in the absence of motion. This is accomplished through coding and manipulating the sensor outputs. By programming the system to adjust the data, any inherent biases or offsets in the sensors are corrected, ensuring that the stationary state consistently reflects a zero measurement. By providing coding efforts, it can also compensate for any potential inaccuracies in the sensor hardware, establishing a reliable starting point for all measurements.

3.4.3 Visualization of Aerodynamic Performance

To analyse the aerodynamic performance for each shape using the vehicle, all data collected is stored and outputted into a CSV file. These files contain key metrics

from each sensor, pressure, airflow and force, respectively to each sensors output. Therefore, each is paired with an exact timestamp for my understanding to locate where the vehicle was located, and thus can be used for later gathering results. The x-axis represents the corner the vehicle is located in and the y-axis corresponds to the sensor-specific unit, which allows an observation of how data changes accordingly when comparing the different angular shapes. When testing occurs, each timestamp is noted to allow a comparison of the data afterwards, along with graphs shown comparing the same sensors with different shapes. Each graph will represent a certain location in the vehicle.

4 Results

Throughout this chapter, all results gathered from all sensors are discussed and analysed based on different angular shapes used. During testing, the vehicle has a top speed of 12 meters per second and an average speed of 9 meters per second. The conditions of the testing session were perfect with sunshine and a temperature ranging from 18°C to 22.5°C, which is of a great importance to ensure that the data gathered can be viable. The results gathered were also compared with simulated results, which were taken prior for understanding if the measurements taken seem applicable, in order to ensure that the data can be used to optimise for specific performance goals. While focusing on the findings gathered and comparing all angular shapes, experimental errors or faults discovered is also discussed. Each graph represents the appropriate measurement in the vertical axis and the turn the measurement is taken in the horizontal axis. Each measurement is plotted while using a timestamp with the vehicle approximately being in that position, give or take 3 to 5 meters. Prior to testing, each corner was noted through timestamps to approximately know upon gathering the results. Using the air friction equation mentioned in section 2.1, we can determine which shape would be the most appropriate.

4.1 Force Sensor Results

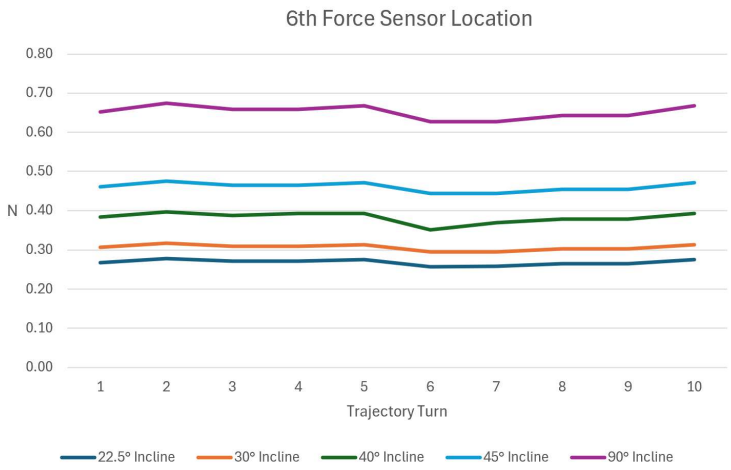

Figure 4.1: Angular comparison of N with the force sensor located on the frontal area of the vehicle

Figure 4.1 shows the Newton variability on each corner, while also graphically showing the different forces each shape drags as they go around the track. From the findings of the above graph, each incline angle has different outputs with the 22.5° outputting the lowest force and the 90° outputting the highest force, due to maximum airflow stagnation.

The 22.5° incline angle ranges from 0.22.58 N to 0.278 N, which reflects low resistance due to a streamlined front. The 30° incline angle ranges from 0.295 N to 0.317 N, indicating a small increase in force as the angle is not much dissimilar. The 40° and 45° angle drag shows a significant rise ranging from 0.369 N to 0.396 N and 0.443 N to 0.475 N, respectively. While of course the biggest difference is the 90° incline angle due to its maximum possible airflow stagnation, the results showcase a drag peak ranging from 0.627 N to 0.674 N, which triples the results found comparing the 22.5° incline angle.

All different incline angles require different motor power to maintain speed, due

to the difference found in drag. This clearly shows that having lower incline angles results in more efficient power and top speed of the vehicle.

4.2 Pressure Sensors Results

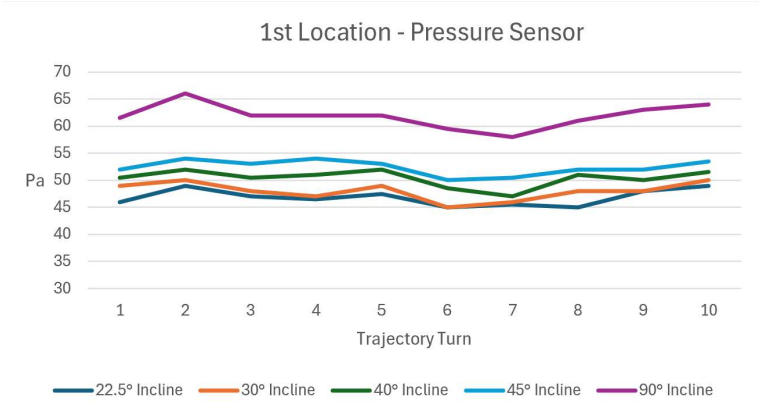

Figure 4.2: Angular comparison of Pa with the pressure sensor located on the front of the vehicle

In Figure 4.2, the front pressure sensor demonstrates the amount of gauge pressure which was found in each corner, while testing the vehicle in different angled shapes. The importance of this result indicates how much pressure was taken, in order to signify power requirements, grip and speed.

When the incline angle of the front pressure sensor was 22.5°, the pressure ranged from 45 Pa to 49 Pa, which indicates moderate stagnation. The 30° incline had quite similar results to the 22.5°, but had stronger stagnation especially in the straights. When comparing both the 40° and 45° incline angles, a greater airflow resistance can be visualised, but both had similar pressures ranging from 47 to 54. The 90° incline had the most pressure, as the shape had a vertical front face, outputting from 58 to 66 Pa.

The results indicate higher pressure in straights overall, with tighter turns 3, 7 and 9 having slightly higher pressure than moderate turns.

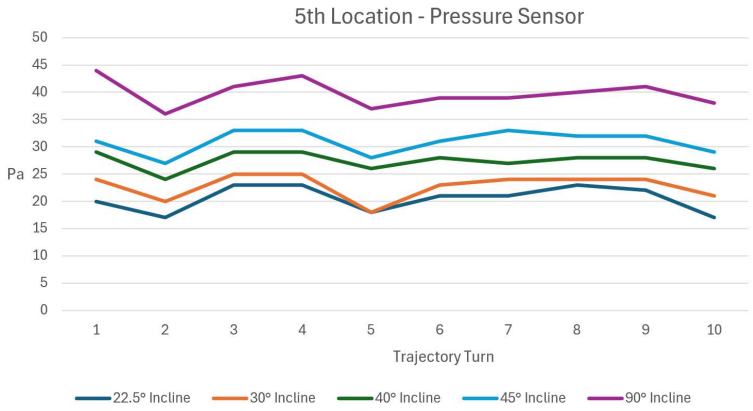

Figure 4.3: Angular comparison of Pa with the pressure sensor located on the top area of the vehicle

While observing at the top of the car shown in Figure 4.3, pressure results in a decrease of Pa, which is found overall while comparing the frontal placed pressure sensor. The top placement is mostly focused on airflow acceleration comparing to the frontal, which focuses more on aerodynamic effects.

The 22.5° incline angle showed results from 18 to 23 Pa, which indicates fast airflow, whereas the 30° incline resulted from 19.5 to 22.5 Pa, with slightly reduced airflow speed. The 40° angle and 45° angle had similar overall results ranging from 24 to 33 Pa, depending on certain turns showing that in turns, it showcases much more pressure than in straights. The 90° incline had much higher pressure than the other angles, but showcased a much higher downforce due to the high amount of pressure when compared.

4.3 Flow Sensors Results

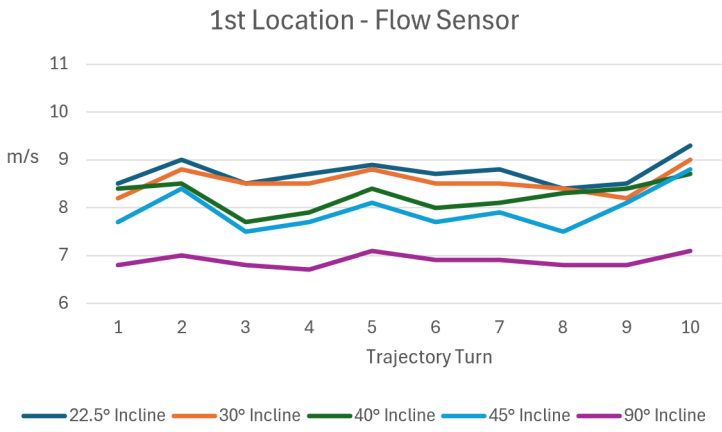

Figure 4.4: Angular comparison of m/s with flow sensor located on front of the vehicle

The results shown in Figure 4.4 collected from the front window flow sensor show airflow velocity decrease, as the incline angle increases, reflecting greater standstill. For the 22.5°, airflow ranges from 8.5 m/s to 9.0 m/s indicating low resistance due to the angular shape. At 30°, the airflow slightly reduces due to a bigger resistance, ranging from 8.3 to 8.8 m/s. The airflow in the 40° and 45° angles are quite similar, with an increase in drag. The airflow of the 90° angle is the lowest naturally, due to the form of the shape. The 90° had much more stability in the turns, compared to the lower angles. From this data, it clearly shows that lower angles are favoured in straight line speeds, whereas the higher the angle, the more stable it becomes in corners.

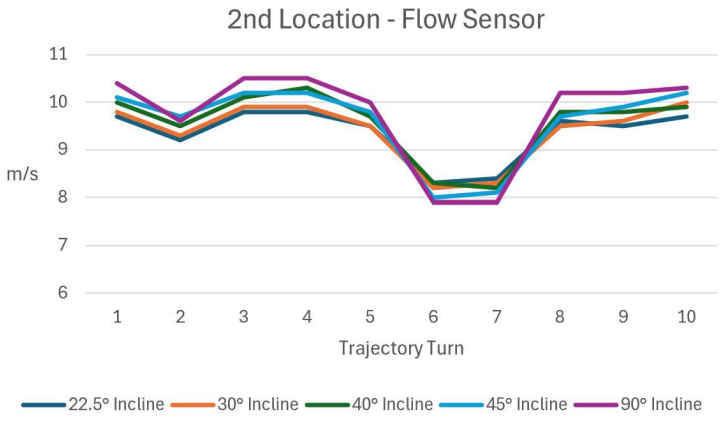

Figure 4.5: Angular comparison of m/s with flow sensor located on the right of the vehicle

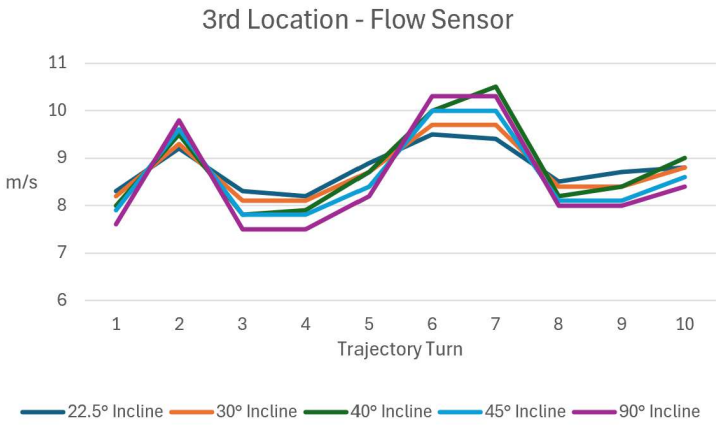

Figure 4.6: Angular comparison of m/s with flow sensor located on the left of the vehicle

When looking at both the right and left flow sensors in Figures 4.5 and 4.6, depending on certain turns, the airflow peaks on the right and left corners, respectively. In turns 1, 3, 4, 5, 8, 9 and 10 which are right, the right flow sensor experiences much higher airflow naturally, whereas left turns located in turns 2, 6 and 7, there is higher airflow in the left flow sensor. Certain outliers can be found when comparing the data, but overall, the higher the incline angle, the higher the airflow in each side

when the vehicle is located in each respective turn. In Turn 4, through the tight right, the right side m/s is higher when the incline angle is 90°. Respectively, in turn 6, which is a left turn, the left side flow sensor shows a higher m/s when the incline angle becomes higher.

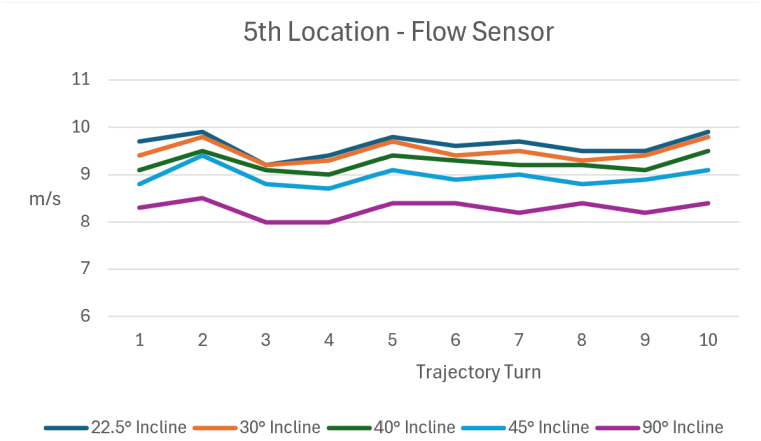

Figure 4.7: Angular comparison of m/s with flow sensor located on top of the vehicle

The top of the vehicle measures airflow related to lift and downforce. When looking at all angles in Figure 4.7, in turn 2 that is through a straight, it indicates fast flow and lift due to high m/s, whereas in tight turns the flow is reduced. Lower angles such 22.5° and 30° are quite suited for speed in Turn 2, while the 90° has the best grip during turn 10 which is a fast paced corner.

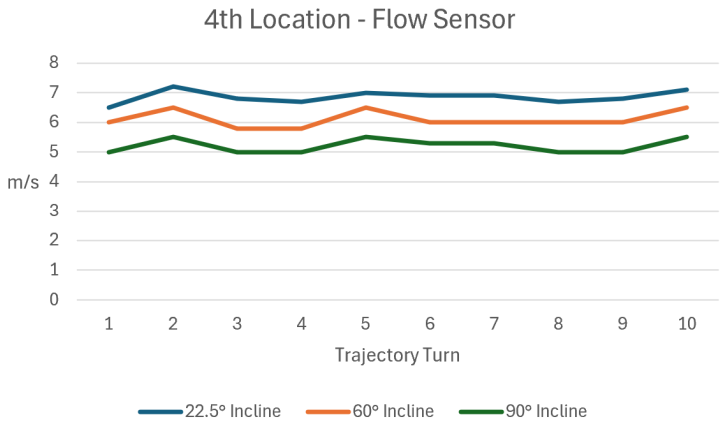

Figure 4.8: Angular comparison of m/s with flow sensor located on the rear of the vehicle

When looking in the slope of the vehicle as shown in Figure 4.8, only three different angles were printed, due to lack of material. The shape models used, which are shown in Chapter 3.3, illustrate the angles of 22.5° which are used once, while the other angles of 60° and 90° are used twice. The graph shows with the lowest angle of 22.5° a much higher flow than the 90° slope. As well, all angles show quite a consistent output in all turns with no major difference throughout the testing session. The back of the vehicle sensor captures quite a low back airflow, but when the vehicle is in a straight such as in turn 2, it has the highest m/s when comparing to other turns.

4.4 Air Friction Results

Using the equation mentioned in section 2.1, a measurement of air friction can be determined as shown in Figure 4.9, using the front flow, force and pressure data. Below, an average of air friction for each incline angle can be illustrated.

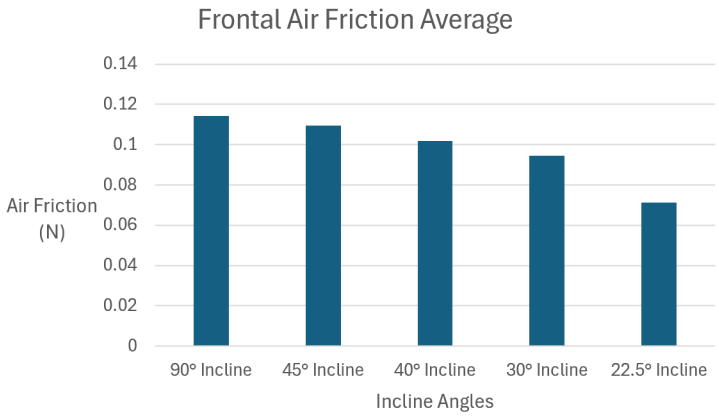

Figure 4.9: Air Friction Results using equation

A significant reduction in air friction when comparing the 90° and 22.5° can be found with a difference of 62%. Each value determines an increase from a lower to a higher incline angle consistently.

4.5 Experimental Errors

Prior to experimenting and conducting the testing session of the above results, simulated data has been generated using a CFD software, to understand and compare the results afterwards between the simulated and real-life testing. Unfortunately, due to tons of technical difficulties, in certain times while testing, the sensors did not provide valid data, due to incorrect placement, disconnection or technical faults. This resulted in inputting assumed data which was checked through the simulation.

In addition, due to the lack of certain parts, multiple tests had to be carried out while using the same parts.

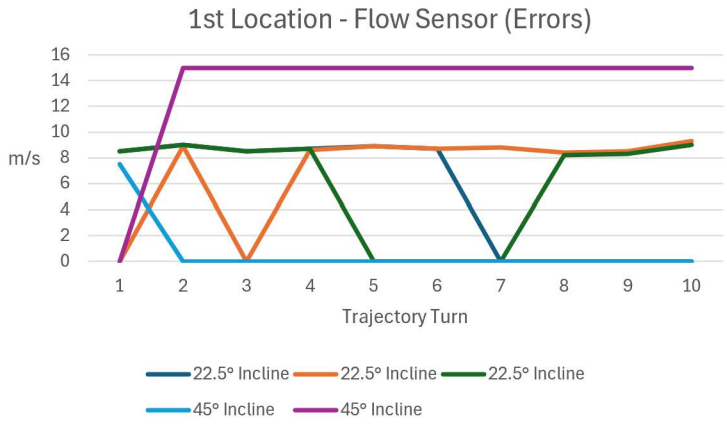

Figure 4.10: Indicating fault outputs due to various technical errors

As seen in the above Figure 4.10, various tests outputted wrong data, illustrating figures having 0 output or too high of a value, which could be due to disconnections or other technical difficulties.

5 Discussion

Throughout this chapter, a thorough discussion regarding the aftermath of completing this thesis is mentioned, from contributions, limitations and future projects which can be achieved from fellow researchers. Even though my main study is regarding robotics and autonomous systems, this project utilises my knowledge in sensors which I gathered while completing my major courses. Knowledge, such as how aerodynamics in vehicles are used, 3D printing, the design process, certain electrical connections, geometrical importance and sensor placement, were all significantly learned during this thesis project. Conclusions regarding the overall thoughts of researching this particular project is discussed, with a thorough view of what could be done in the future.

5.1 Summary of findings

Comprehensive data regarding airflow, pressure and force was found when considering how the different incline and rear slope angles affect performance. The airflow sensor results indicate that front window airflow at a 22.5° angle, has a higher drag at steeper front inclines, especially when noticing the turn 2 findings where speed peaks. Right window airflow peaks at right turns, whereas left window airflow peaks at left turns, respectively, highlighting stability differences, amplified at 90°. Top airflow is highest when the incline angle is at 22.5°, which suggests lift, whereas the

lowest at 90° indicates downforce. The airflow sensor located at the back provides the lowest output, showing that it has the largest wakes, leading into an increased drag. Both pressure sensors had significant values, reflecting stagnation for the front and the top, indicating lift when comparing the results from smallest angle to largest, respectively. The force sensor shows that there is a higher grip when the incline angle is at 90° and at 22.5° it minimizes drag for speed. Real world complexities were a key reason in the reasoning of gathering data, with each test illustrating a valid and calibrated simulation.

5.2 Contributions to this Thesis

The idea of this thesis started with the passion in vehicle engineering and design, with also the possibility to further understand how certain design aspects can influence efficiency and drag. The scale of the vehicle is small, so undoubtedly there is a significant difference when engineering and drag is considered, with normal scaled sized vehicles, including huge weight differences that depend on size and shape.

The vehicle used for this project was already used for prior research in other matters, and was mainly constructed together from Abdul Malik, which he exceptionally assisted in the possibility of completing the research for this thesis. Furthermore, assistance was also provided in the usage of the Jetson Nano, as well as designing 3D printing material. This project would have not been successfully accomplished without the input of the designated supervisors, along with the possibility in using equipment from the university.

5.3 Limitations

Many types of limitations were faced while conducting the practical work for this thesis, from 3D printing to electronic fault. Certain printing material was required for certain printers and it became difficult and time-wasting in finding a suitable printer which would print these shapes, whilst considering the average length of each print taking up to two days. Unfortunately, some printing material was wasted due to faulty equipment found within the printer, with wasted time becoming of essence when it was time to conduct the test. The sensors used were suitable but very sensitive, and certain connections had to be made proper, as disconnections were very easy due to the motion of the vehicle. The pressure and flow sensors were easily breaking due to overheating and the connections were quite fragile, along with the tips of the pressure points being easily breakable. The consistent state of the sensors staying in the same place was a tough challenge even if they were placed with tape, as the motion of the car from a road hump might disconnect some sensors while conducting the tests.

5.4 Future Projects

Several promising directions for future research with this project, provide a robust foundation that can be achievable using this study as a basis. As such, some limitations were found during the working process, and certain ideas could not be inputted, due to constraints in time or resource. This section will focus on suggestions for improvements and possible projects that can be attributed from a continuation perspective of this thesis.

(1). The possibility of autonomous driving around a small track while it holds constant speed, would be an ideal take in achieving better outputs. A better version of the Jetson Nano which is able to hold and collect data from more sensors than the current one, could result in more sensors being placed around the vehicle and acquiring better data overall.

(2). Due to the lack of material for printing, more exploration can be established within findings in focusing on even more further advanced shape optimizations. An adjustable rear spoiler for downforce and drag data would be an interesting concept in understanding balancing speed and grip when optimizing spoiler settings.

(3). Another further advanced shape optimization would be adding side winglets on the vehicle's flanks to generate data on lateral aerodynamic forces. Force sensors on both sides can measure sideways forces and velocity can be more accurately captured using those flanks.

(4). Underbody airflow effects would be an interesting concept to understand and explore how different angles and distance from the floor contribute to a different velocity and pressure, where a sensor of both can obtain what would be the ideal use in specific turns or straights.

(5). Sensors for battery and motor efficiency with those different angles can show how much efficient a vehicle becomes. This can lead to understanding further which battery is appropriate, and how much energy is required for each shape.

(6). An implementation of a dynamic incline adjustment system, which might have difficulties to be achieved, would be a fascinating input to gather real-time

data on adaptive aerodynamics. From this, data from each corner would be interesting to see when it comes to optimize performance.

(7). Surface material variations can alter wake characteristics, with textured and smooth surfaces providing different data. Different types of surface material might show different efficiency due to different weight.

(8). Different temperature and altitude can vary the data gathered, which would be an interesting take, considering how all sensors would be affected regarding different conditions.

(9). An interesting approach to expand on this current project is seeing how smooth and efficient the vehicle becomes under wet conditions, while focusing on the vehicle having good grip.

(10). A stronger engine can output higher performances in the RC vehicle, and therefore match closer to the real life scaled auto mobile. Higher speeds in corners and straights can produce altered data, with each sensor illustrating similar patterns in force and flow.

5.5 Conclusion

While the results might not satisfy fully, due to the lack of time, equipment and a scaled real life car model, it provided an opportunity to learn and understand new concepts that would satisfy the future of work in the automotive vehicle industry.

Rather than being able to use a full scaled vehicle, it allowed the possibility of using a small model to 3D print small scaled shapes that were placed on top of

the RC. The results showed promising numbers that acknowledge factors that were already proven, but throughout this research, a more thorough practical work took place. The design process in each vehicle proves that it is very important to consider all angular factors. From efficiency to high speeds, each model is unique with its own parameters, as well as focusing on how effective in energy a vehicle becomes, especially if it is used properly from a day-to-day basis.

Each vehicle manufacturer has its own goals in mind considering the design of the car, while also satisfying customer needs, from looks to drivability. Different roads around the globe consist of different environmental factors, with grip and vehicle stability becoming important for vehicle safety, showing that each vehicle design is unique and appropriate to certain roads and environments.

References

[1] Y. Fu, "Aerodynamics and drag of a car", 2023. [Online]. Available: https://www.researchgate.net/publication/370575425_Aerodynamics_and_Drag_of_a_Car.

[2] R. Sterner, "The conservation of mass", 2011. [Online]. Available: https://www.nature.com/scitable/knowledge/library/the-conservation-of-mass-17395478/.

[3] NASA, "Navier-stokes equations", 2015. [Online]. Available: https://www.grc.nasa.gov/www/k-12/airplane/nseqs.html.

[4] Britannica, "Conservation of energy", 2018. [Online]. Available: https://www.britannica.com/science/conservation-of-energy.

[5] J. Anderson, "Introduction", in *Governing Equations of Fluid Dynamics*, 2009, p. 1. [Online]. Available: https://www.eng.auburn.edu/~tplacek/courses/fluidsreview-1.pdf.

[6] J. Anderson, "2.8.4 boundary conditions", in *Governing Equations of Fluid Dynamics*, 2009, p. 30. [Online]. Available: https://www.eng.auburn.edu/~tplacek/courses/fluidsreview-1.pdf.

[7] C. CFD, "Solving the navier-stokes equations in fluid mechanics", 2022. [Online]. Available: https://resources.system-analysis.cadence.com/blog/msa2022-solving-the-navier-stokes-equations-in-fluid-mechanics.

[8] N. Hall, "First law of thermodynamics", 2021. [Online]. Available: https://www.grc.nasa.gov/www/k-12/airplane/thermo1.html.

[9] "Fs7 documentation", in *FS7.0.1L.195*, innovative Sensor Technology. [Online]. Available: https://www.ist-ag.com/sites/default/files/downloads/fs7.0.1l.195.pdf.

[10] P. V. N. Kai Siren Gunnar Rosén, "Experimental techniques", in *Industrial Ventilation Design Guidebook*, 2001.

[11] "Pressure sensors documentation", in *Board Mount Pressure Sensors*, Honeywell, p. 20. [Online]. Available: https://mm.digikey.com/Volume0/opasdata/d220001/medi%20as/docus/1808/HSC_DS.pdf.

[12] S. P. G.M. Kim, "Piezoresistive sensor", in *Composite Structures*, 2019. [Online]. Available: https://www.sciencedirect.com/topics/engineering/piezoresistive-sensor.

[13] T. Connectivity, "Load cell documentation", in *FX19 Compression Load Cell*, 2020. [Online]. Available: https://www.te.com/commerce/DocumentDelivery/DDEController.

[14] L. V. Vilamajo, "How very low ambient temperatures impact on the aero of wrc cars", 2021. [Online]. Available: https://www.wrcwings.tech/2021/02/15/how-very-low-ambient-temperatures-impact-on-the-aero-of-wrc-cars/.

[15] J. D. A. Jr., "Equations", in *Fundamentals of Aerodynamics*, 2011, p. 956.

[16] J. D. A. Jr., "Necessary thermodynamic background", in *Fundamentals of Aerodynamics*, 2011, p. 691. [Online]. Available: https://archive.org/details/FundamentalsOfAerodynamics5thEdition.

[17] J. Williams, "Understanding air density and its effects", [Online]. Available: https://iflycoast.com/understanding-air-density-and-its-effects/.

[18] J. D. A. Jr., "Flow velocity and streamlines", in *Introduction to flight*, 2008, p. 58.

[19] L. I. Brúnó Péter, "Analysis of the aerodynamic parameters of road vehicles affected by weather conditions", [Online]. Available: https://www.cetjournal.it/index.php/cet/article/view/CET24114173.

[20] T. B. et al, "Effect of surface roughness on the aerodynamic performance of turbine blade cascades", [Online]. Available: https://www.sciencedirect.com/science/article/pii/S2212540X1%204000194.

[21] M. V. Florian Hau Florian Baumgärtner, "The degradation of automotive radar sensor signals caused by vehicle vibrations and other nonlinear movements", 2020. [Online]. Available: https://www.mdpi.com/1424-8220/20/21/6195.

[22] L. J. Grip H.F. Imsland, "Estimation of road inclination and bank angle in automotive vehicles. in 2009 american control conference", 2009. [Online]. Available: https://ieeexplore.ieee.org/abstract/document/5159912/.

[23] P. University, "Bernoulli's equation", 1997. [Online]. Available: https://www.princeton.edu/~asmits/Bicycle_web/Bernoulli.html.

[24] M. T. S. Pal S. Kabir, "Aerodynamic analysis of a concept car model", 2015. [Online]. Available: https://www.cuet.ac.bd/icmere/ICMERE%202015%20Proceedings/Session-IV(D)/ICMERE2015-PI-282.pdf.

[25] P. J. Malik Abdul Haghbayan Hashem, "Run-time modelling of energy consumption in mobile robots : Technical report - 2024", 2024. [Online]. Available: https://www.utupub.fi/handle/10024/178992.

[26] RBR, "Track used for testing", *Red Bull Ring History*, 1969. [Online]. Available: https://www.redbullring.com/en/.